USING AN INTEGRATED HYDROLOGY MODEL TO ELUCIDATE PLANT WATER USE IN A HEADWATERS RESEARCH CATCHMENT

by

Caitlin M. Collins

A thesis submitted to the Faculty and the Board of Trustees of the Colorado School of Mines in partial fulfillment of the requirements for the degree of Master of Science (Hydrologic Science and Engineering).

Golden, Colorado

Date _____

Signed: _____
Caitlin M. Collins

Signed: _____
Dr. Reed Maxwell
Thesis Adviser

Golden, Colorado

Date _____

Signed: _____
Dr. Kamini Singha
HSE Director

ABSTRACT

Mountain headwaters are vulnerable to change. Increases in annual average temperature, changes in seasonal precipitation and drought stress will continue to alter the dynamics of these delicate ecosystems. Despite its significance in the water budget, both the quantity and partitioning of evapotranspiration (ET) is poorly resolved. Restricted by discrete point observations, physical observations in mountain headwaters are challenging, limited by uncertainties and difficult to scale. Integrated, physically-based models are tools for dissecting the mechanisms driving evaporation and transpiration. Understanding mountain vegetation water use is an essential component for predicting the vegetative response to stress. This study is motivated by evidence of drought-induced tree mortality in some Sierran catchments, a high degree of uncertainty in mountain regolith groundwater storage, and the impacts of subsurface characterization on mountain ecohydrology (Holbrook et al. 2014; Jepsen et al. 2016). Using a physically-based integrated modeling approach, this study explores the role of lateral groundwater flow on the drought-tolerance of montane vegetation. Despite a 68.8% decrease in precipitation during the drought period, evapotranspiration only decreased by 26.5%. From the pre-drought period to the drought period the total change in groundwater storage decreased by 470%. Incorporating lateral groundwater flow increased transpiration partitioning (T/ET) from 44.9% to 59.0% in the pre-drought period and from 52.8% to 63.5% in the drought period. These results suggest that plant stress is mitigated under drought conditions because lateral flow of groundwater storage sustains transpiration.

TABLE OF CONTENTS

ABSTRACT……iii
LIST OF FIGURES……v
LIST OF TABLES……vi
ACKNOWLEDGMENTS……vii
CHAPTER 1 INTRODUCTION ……1
1.1 Study Site……2
CHAPTER 2 INTEGRATED MODELING APPROACH ……5
2.1 Model Development ……6
2.2 Meteorology ……8
2.3 Model Initialization ……9
2.4 Model Simulations ……9
CHAPTER 3 RESULTS……12
3.1 Water Balance……12
3.2 Critical Zone Relationships with Water Table Depth……14
3.3 Evapotranspiration through the recent California Drought……15
3.4 Lateral Groundwater Flow on Transpiration through the California Drought……19
CHAPTER 4 CONCLUSION ……22
REFERENCES CITED……24
APPENDIX ……29

LIST OF FIGURES

Figure 1.1 Providence Creek watershed (P300) ……..……..……3

Figure 2.1 Hydrology modeling……..……5

Figure 2.2 Building a ParFlow-CLM model from complex datasets…….6

Figure 2.3 P300 precipitation and air temperature at a glance before and during the drought..……..……..……...9

Figure 3.1 Simulation P300 water balance……..……..……..12

Figure 3.2 Annual P300 water balance ...…..……..……13

Figure 3.3 Evapotranspiration (ET) relationships with water table depth (WTD)……..14

Figure 3.4 Visualizing evapotranspiration spatially for the base case model……16

Figure 3.5 The sensitivity of water table depth (WTD) to subsurface characterization ……..……..……..……18

Figure 3.6 The effect of lateral groundwater flow on transpiration partitioning (T/ET) ……..……..……..……20

Figure A.1 Original and adjusted NLDAS-II precipitation..……..……29

Figure A.2 Visualizing the subsurface sensitivity study ..……..……..30

Figure A.3 Visualizing evapotranspiration spatially for subsurface sensitivity study……..……...……..31

Figure A.4 Total annual average water table depth (WTD) for subsurface sensitivity study……...……..……..…...33

LIST OF TABLES

Table 3.1 Total Annual Evapotranspiration (ET) Components, Water Balance Components, and Runoff Ratios for Pre-drought and Drought Periods……17

ACKNOLEDGEMENTS

Data available from the U.S. Geological Survey. See USGS Visual Identity System Guidance (link is external) for further details.

This research was funded by Lawrence Livermore National Lab LDRD project 15-ERD-042.

CHAPTER 1
INTRODUCTION

The 2012-2017 drought was the driest period in California record-keeping (U.S. Geological Survey 2017). Parts of the Southern Sierra Nevada experienced a 70% reduction in precipitation from 2011 to 2012. In the Southern Sierras, tree-mortality was observed as a direct response to this recent drought. In the Southern Sierras, catchments above 1000 m are dominated by snow in the winter. Increasing average annual temperature forces the rain-snow transition line to higher elevations thereby reducing snowpack duration and volume. The ecohydrologic relationships between subsurface water storage and plant water stress with changing climate regimes in these systems are especially important. Spring snowmelt provides vegetation with the necessary plant-available water for the growing season (Bales et al. 2014). Since snowpack is a critical driver of streamflow and soil moisture in mountain systems, reductions in snowpack duration and volume directly affect the extent and vitality of the plant growing season (Blankinship et al. 2014; Beniston 2003).

As the largest terrestrial flux, it is critical to bracket evapotranspiration (ET) estimates to inform downstream water management and planning with an accurate water balance of these complex mountain systems (Trenberth et al. 2007). Evapotranspiration is difficult to estimate in the field. Currently, evapotranspiration estimates are sourced from point observations at eddy covariance flux towers. Installation of instrumentation is often location dependent and limited by both internal (i.e. poor calibration and metadata documentation) and external (i.e. environmental challenges and equipment malfunction) sources of error. Scaling these point data is difficult as evapotranspiration depends on spatially heterogeneous factors such as vegetation, soil and geology, and energy inputs.

Providence Creek (P300) watershed is a heavily instrumented alpine headwaters catchment located at the Southern Sierra Critical Zone Observatory (SSCZO). Observations at P300 show depleted plant available water in the soil column early into the growing season and deep reaching root systems (Hubbert, Graham, and Anderson 2001). During wet years, shallow water table depths enable both deep and superficial root networks access to groundwater. Conversely, in dry years, decreased precipitation

reduces water table levels thereby drastically reducing the zone of drought-tolerant vegetation. This response is especially pronounced under sustained drought.

Physically-based hydrology models provide an avenue for studying process interactions and system behavior to climate perturbations. There is a proliferation of work documenting the relationships between evapotranspiration (ET) and water table depth (WTD) (Condon, Maxwell, & Gangopadhyay, 2013; Kollet & Maxwell, 2008a; Maxwell & Kollet, 2008). Although it is still unclear exactly how much water vegetation is using, recently Maxwell & Condon (2016) demonstrated the significant role of lateral groundwater flow on evapotranspiration partitioning at the continental scale (Maxwell and Condon 2016). Recent work suggests Sierran vegetation is sustaining ET under water stress hypothesizing that plants are accessing deeper groundwater storage (Bales et al. 2018). However, little research has focused on the ecohydrologic relationships between montane groundwater flow and plant water stress under sustained drought. Using ParFlow-CLM, this study assesses the importance of lateral groundwater flow on subsurface water storage and plant water stress, as well as brackets evapotranspiration estimates, during drought conditions in a headwaters system at the watershed scale.

1.1 Study Site

Providence Creek (P300) watershed is an alpine headwaters catchment located in the Southern Sierra Nevada mountains, approximately 50 miles east-northeast of Fresno, California (Figure 1.1A). Nested within the Kings River Experimental Watershed (KREW), P300 converges with Big Creek and eventually feeds into the Pine Flat Lake to the south. P300 is one of four heavily instrumented research catchments at the Southern Sierra Critical Zone Observatory (SSCZO). The Critical Zone Observatory (CZO) network is a conglomerate of hypothesis-based research funded by the National Science Foundation (NSF) at eleven locations across the United States and Puerto Rico (National Science Foundation 2016b). The primary goal of the CZO network is to use an interdisciplinary approach to study the critical zone—the dynamic region of the Earth's crust between the bedrock and the vegetative canopy—by integrating observations and

modelling efforts to elucidate biologic, geologic, hydrologic, and atmospheric interactions across spatiotemporal scales (National Science Foundation 2016a).

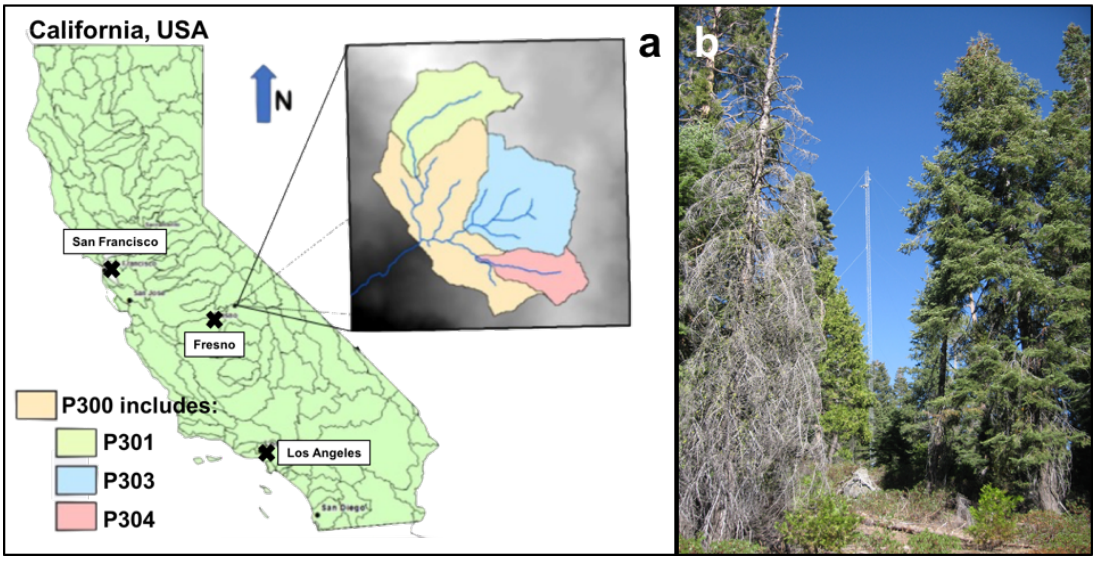


Figure 1.1 Providence Creek watershed (P300): (a) location of study site and included sub-watersheds; (b) Example of tree mortality at P301 eddy covariance flux tower. Picture taken by Southern Sierra Critical Zone Observatory (SSCZO).

P300 covers roughly 4.5 square kilometers of lodge pole pines and mixed shrubbery with intermittent bare rock outcrops. Three smaller sub-catchments—P301, P303, and P304—are included in P300 (Figure 1.1A). P300 experiences a Mediterranean climate year-round which, in central California, translates to wet winters and dry summers (Kelly and Goulden 2016). The Providence Creek watershed receives between 150 cm and 200 cm of precipitation each year (Liu, Hunsaker, and Bales 2013), mostly during the winter months, the majority of which falls as snow in the mid- to high-elevations (Safeeq and Hunsaker 2016).

Elevations at Providence Creek range between 1660 m and 2115 m above sea level (Southern Sierra Critical Zone Observatory 2016). This 455 meter variation translates to average annual temperatures of 6˚C to 7˚C at the bottom of the catchment to 8˚C near the top of the catchment (Southern Sierra Critical Zone Observatory 2016). Wind speeds rarely surpass 1 ms^{-1} to 2 ms^{-1} (Southern Sierra Critical Zone Observatory 2016). Wind directions generally move downslope during the day and upslope at night (Southern Sierra Critical Zone Observatory 2016).

One of the goals of the SSCZO at P300 is to understand how the regolith plays a role in the local ecohydrology—namely the vegetative response to hydrologic regimes in the subsurface, such as the groundwater (National Science Foundation 2016c). Regolith is defined as the loose, heavily weathered, and sometimes unconsolidated, superficial material overlying less weathered bedrock of the same geologic history (Graham, Tice, and Guertal 1994). The regolith subsurface layer is more broken up than the underlying bedrock and feeds the supply of soil. Tree roots take advantage of the highly chemically weathered and more easily fractured regolith (Graham, Tice, and Guertal 1994; Holbrook et al. 2014). Accurate characterization elucidates subsurface water storage. Figure 1.1B depicts the dichotomy between healthy and water-stressed vegetation at the P301 eddy covariance flux tower. Understanding water availability and vegetative accessibility will illuminate process interactions during environmental stressors (i.e. drought conditions and land cover changes).

CHAPTER 2

INTEGRATED MODELING APPROACH

ParFlow (PF) is a physically-based integrated hydrologic model that solves the three-dimensional Richards equation and the two-dimensional kinematic wave equation to simulate variably saturated subsurface and surface flow condition (Figure 2.1B) (Jones and Woodward 2001; Kollet and Maxwell 2006). When coupled to the Common Land Model (CLM), PF-CLM can simulate land surface processes, including a complete land-energy balance and snow dynamics, while accounting for evapotranspiration (Kollet and Maxwell 2008b; Maxwell and Miller 2005; Dai et al. 2003; Jefferson and Maxwell 2015; Jefferson et al. 2015; Ferguson et al. 2016). Parallel implementation provides solver efficiency for complex problems (Ashby and Falgout 1996; Osei-Kuffuor, Maxwell, and Woodward 2014; Kollet et al. 2010; Maxwell 2013).

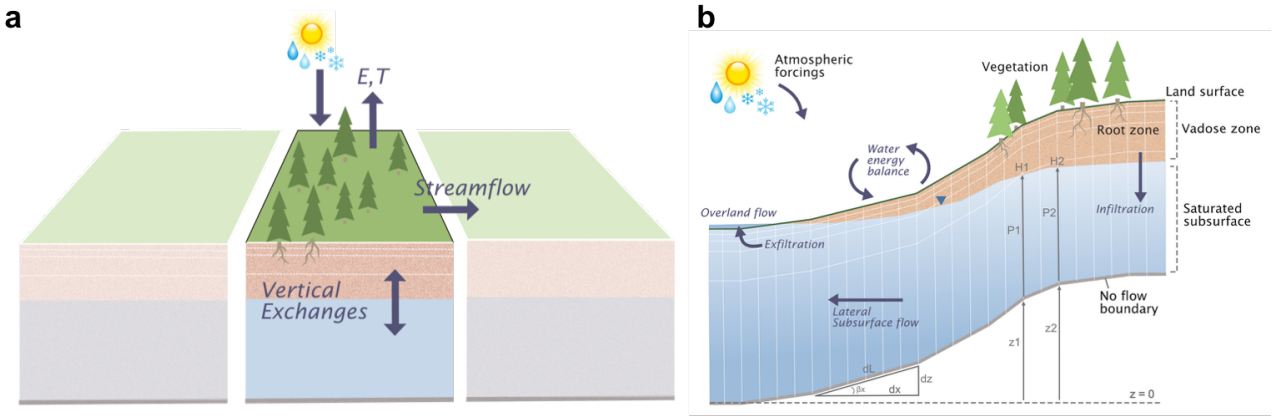


Figure 2.1 Hydrology modeling: (a) traditional land surface model with only vertical exchanges; (b) ParFlow model including lateral flow.

Unlike traditional land surface models, which only allow vertical exchange of water, ParFlow uniquely incorporates lateral groundwater flow (Figure 2.1). Additionally, ParFlow does not require a pre-defined stream network but rather allows streams to form organically from topographical variations. The flexibility of ParFlow allows the user to mimic traditional groundwater models by turning off lateral groundwater flow and terrain-following grid capabilities.

2.1 Model Development

Site characterization was developed from available complex datasets, such as topography (Figure 2.2A), land cover (Figure 2.2B), soil (Figure 2.2C) and geology (Figure 2.2D) and are implemented onto a computational grid. All input datasets were projected into the NAD 83 zone 11 coordinate reference datum and resampled to a 100-meter resolution using ArcMap 10.3.1 software. Following additional processing with GRASS GIS 7.0.4 software, x- and y-directional slopes were processed from a 1/3 arc-second digital elevation model (DEM), obtained from the Lawrence Livermore National Lab (LLNL) (Figure 2.2A).

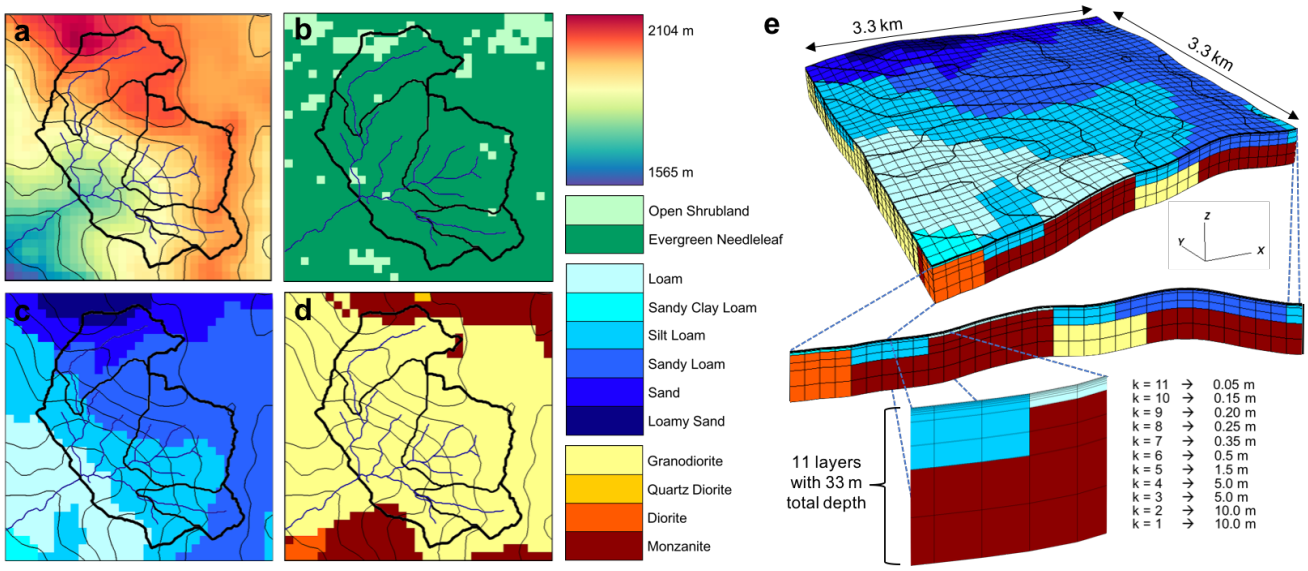


Figure 2.2 Building a ParFlow-CLM model from complex datasets: (a) digital elevation model (DEM); (b) NLCD land cover data; (c) SSURGO soil data; (d) USGS geology data; (e) developing and implementing datasets onto a computational grid.

Subsurface characterization is developed from available soil and geologic datasets. Soil texture, hydraulic parameters, and spatial variability were obtained from the Natural Resources Conservation Service Soil Survey Geographic database (SSURGO) (Figure 2.2E) (Soil Survey Staff, Natural Resources Conservation Service 2017). This data was pre-digitized and interpolated to the 100-meter grid. A total of six soil types were identified. Regions of rocky outcrops within the soil data were replaced with underlying geology. Geologic data was obtained from the United States Geological

Survey (USGS) National Geologic Map Database (Figure 2.2D) (Bateman and Wones 1972). Soil layers are confined to the upper five vertical layers—making up the top two meters—of the subsurface. However, three-dimensional heterogeneity of the five soil types and four geology types within the upper five layers was mapped using additional SSURGO-derived data. Cells above a SSURGO-defined hydraulically-restrictive horizon were identified as soil and those below as geology (Soil Survey Staff, Natural Resources Conservation Service 2017). As a lower no-flow boundary condition, impermeable bedrock is assumed below the geology. The overland-flow boundary condition was applied to the top surface. Constant flux boundary conditions were established on the remaining sides of the domain. A homogeneous specific storage of 1.0×10^{-5} m^{-1} is assigned for the domain.

Land cover data was obtained from the National Land Cover Database (NLCD) 2011 release, which is derived from 2006 Landsat imagery (Figure 2.2B) (Homer et al. 2015). Seven land cover types were identified. Of the domain's 11.4 square kilometers, 89% is forested and 11% is scrubland. In addition to characterizing the Manning's coefficients (surface roughness) for ParFlow, land cover data informs CLM with a variety of vegetative parameters (Homer et al. 2015).

Developing the computational grid involves balancing the computational expense with process interaction resolution and depends heavily on the nature of the scientific question being asked. Figure 2.2E depicts how variations in soil and geology of the base case are implemented onto the computation grid. Figure 2.2E also shows variations in the characterization and vertical discretization. The Providence Creek watershed (P300) domain consists of 33 rows, 33 columns, and 11 layers ranging from five centimeters at the surface to 10 meters within a terrain following grid framework (Figure 2.2E). The total computational grid is defined by 11,979 cells over a 11.4 km^2 horizontal extent. An extensive vertical discretization extending 33 meters into the subsurface resolves near-surface fluxes (i.e. evapotranspiration) while capturing the lateral movement of groundwater. Extending the boundaries of the domain beyond the P300 catchment and implementing constant flow boundary conditions relaxes assumptions.

2.2 Meteorology

PF-CLM simulates a complete land-energy budget but requires forcing at high temporal resolution (~hourly) for the following atmospheric variables: air temperature [K], precipitation [mms^{-1}] surface pressure [Pa], specific humidity [$kgkg^{-1}$], downward longwave and shortwave radiation [Wm^{-2}], and wind speed in both the east-west and north-south directions [ms^{-1}]. As only daily observations of some of these variables were available, the model was driven with reconstructed meteorology from the North American Data Assimilation Survey phase II (NLDAS-II) data product (Mitchell et al. 2004; Cosgrove et al. 2003). Through vegetation, these variables allow a dynamic calculation between the land and atmosphere. Not only does the climate forcing data impact model outputs, such as runoff, snowpack, and energy fluxes, but it also informs model initial conditions.

Initial simulations using the NLDAS-II meteorology resulted in underestimated discharge at Providence Creek. The underestimated flows are a direct implication of downscaling a large-scale data product, such as the 32 km^2 NLDAS-II product, to a higher resolution grid. The NLDAS-II precipitation was adjusted by 30% to match observations at the Upper and Lower Meteorological (MET) stations at P300. Figure A-1 shows how the adjusted NLDAS-II precipitation is better represented at both MET stations.

2012 through 2017 is one of the driest periods in California history (U.S. Geological Survey 2017). Figure 2.3 explores the temporal changes in precipitation and air temperature in the pre-drought period (light blue shading) and drought period (light red shading). The dark blue bars represent the total accumulated precipitation (from NLDAS-II data product) that fell each pre-drought year at P300. The light blue bars represent the total accumulated precipitation (also from NLDAS-II data product) that fell during each drought year at P300. The yellow and red symbols represent the average air temperature each year at P300 in degrees Celsius.

Providence Creek (P300) watershed saw a 61.7% average decrease in precipitation during the drought period and a six percent average increase in air temperature (Figure 2.3). The temporal precipitation and temperature trends from NLDAS-II (Figure 2.3) agree with California records.

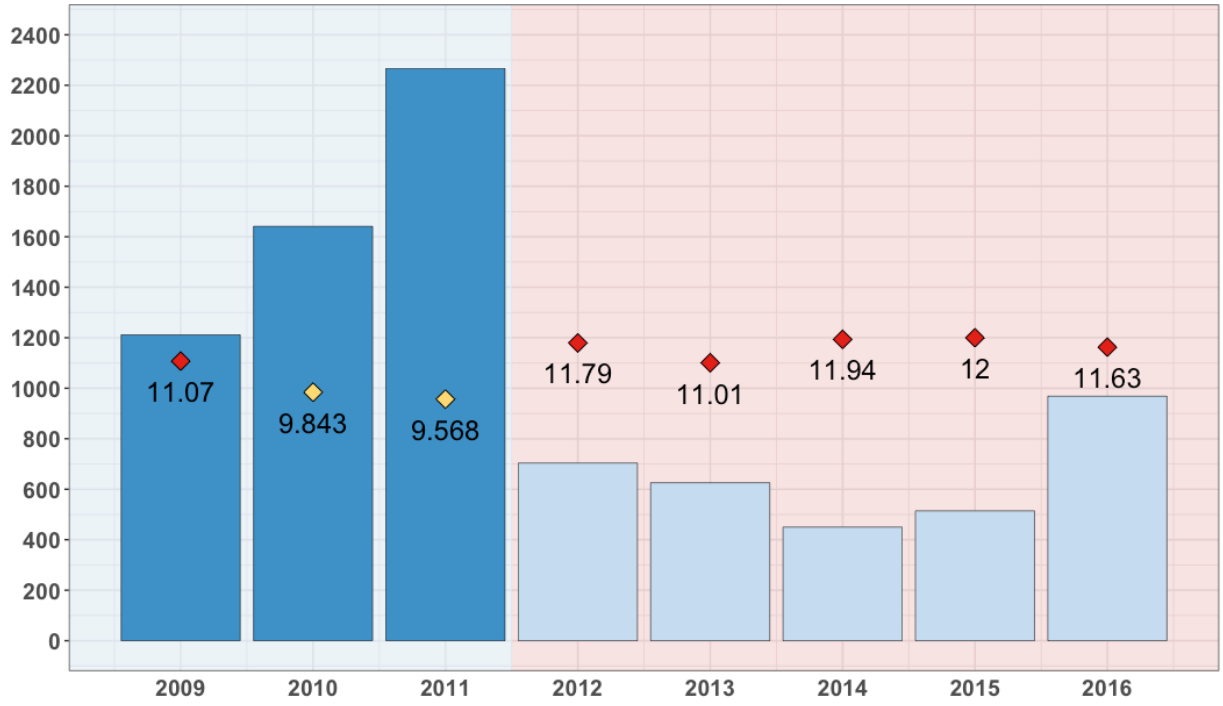


Figure 2.3 P300 precipitation and air temperature at a glance before and during the drought.

2.3 Model Initialization

The model spin-up phase—the process of achieving dynamic equilibrium of subsurface and surface fluxes—establishes an initial pressure field for the simulation period. This process is two-fold. First, the ParFlow model was driven with a long-term averaged precipitation minus evapotranspiration (PME) value for 80 years to establish groundwater. Then driven with NLDAS-II forcing from water year 2009 with CLM for an additional 20 years to establish land-surface processes. Dynamic steady-state is reached when the change in subsurface storage with respect to recharge is less than one percent. The purpose of the model spin-up phase is to ensure the effects of any initial conditions are removed and that responses of the system can be attributed to perturbations (i.e. drought conditions) in the simulation.

2.4 Model Simulations

Subsurface characterization at Providence Creek watershed (P300) is uncertain. Recent studies suggest that vegetation rooting depths at P300 may be as deep as 15

meters (Holbrook et al. 2014). Integrated modeling in conjunction with observations is a tool for bracketing subsurface characterization. In this study, a sensitivity analysis was conducted to understand the impact of subsurface parameter uncertainty on model estimated fluxes. This sensitivity analysis brackets a low effective domain permeability with a high effective domain permeability. In addition to the base case model (Figure A-2A), three additional model characterizations were developed: a homogeneous geology subsurface (Figure A-2C), a double permeability subsurface (Figure A-2D), and a quadruple permeability subsurface (Figure A-2E).

Figure A-2 depicts the differences in the soil and geology hydraulic conductivities across the different model characterizations. The homogeneous subsurface model has identical soil properties and spatial variability as the base case model but with a single geology (Figure A-2C). The double and quadruple permeability cases have identical soil and geology spatial variability as the base case model except the hydraulic conductivities are doubled and quadrupled, respectively. Table 3.1 provides an overview of the total annual evapotranspiration components, precipitation, discharge, and changes in storage as annual averages for the pre-drought period (2009-2011) and the drought period (2012-2016) for all five models. Meteorology was held constant across all model simulations.

A free-draining model variation (Figure A-2B) of the P300 domain was created to explore the role of topographically-driven lateral groundwater flow on plant water stress. By simply turning off lateral groundwater flow in ParFlow, a land surface model is simulated. The surface and subsurface properties of the free-draining model are identical to the base case model. Figure 2.1 depicts the conceptual differences between traditional land surface models and ParFlow. The primary difference being lateral groundwater flow.

Following the spin-up phase—80 years of steady-state and 20 years of transient simulation—all five model variations were run at an hourly time step over a simulation period from 2009 through 2016, effectively capturing a normal to wet pre-drought period, the recent California drought, and the beginning of drought-recovery. For the purpose of analysis, the “pre-drought” period is defined as water year 2009 through

2011 simulation years and the “drought” period is defined as water years 2012 through 2016 simulation years.

CHAPTER 3

RESULTS

3.1 Water Balance

Figure 3.1 is an unconventional visualization of the water balance for P300 but provides a general overview of P300 catchment behavior for each simulation year. The purple bars are the total precipitation [mm] input, the blue bars are the total discharge [mm] at the P300 outlet (represented as a positive value in this figure), the green bars are the total evapotranspiration [mm] in P300, and the red bars depict the total change in storage [mm] over each simulation year. Distinct pre-drought and drought periods form. Despite a significant decrease in precipitation through the drought period, the magnitude of evapotranspiration is maintained. Figure 3.1 provides insight into the mechanism sustaining the vegetation which is plant-accessible groundwater storage by lateral groundwater flow.

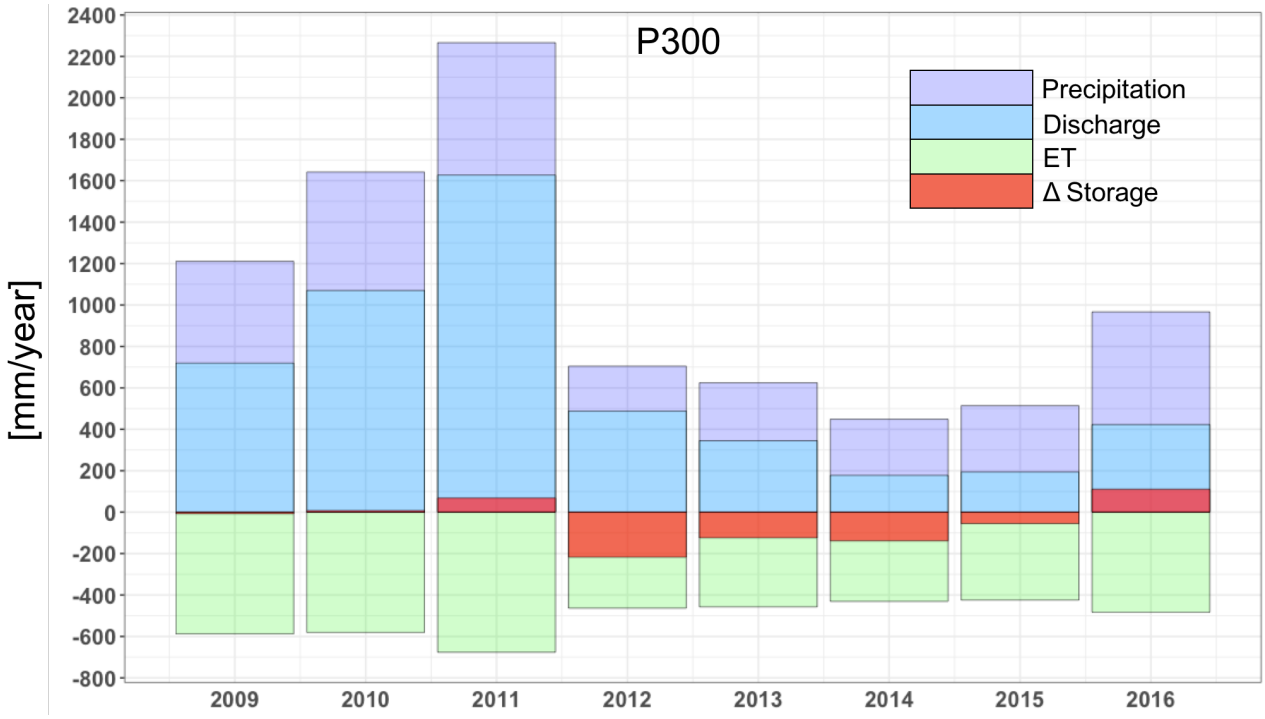


Figure 3.1 Simulation P300 water balance. Total precipitation is represented by the purple bars, total discharge is represented by the blue bars, total evapotranspiration is represented by the green bars, and total change in storage is represented by red bars.

Figure 3.2 depicts a cumulative water balance for 2011—a pre-drought year (Figure 3.2A)—and 2014—a drought year (Figure 3.2B)—for the P300 watershed for the base case simulation, where the purple shaded region represents cumulative precipitation over the year, the blue shaded region is the cumulative flow at the P300 outlet, and the black dots represent the point in time where precipitation or snowmelt ceases for the year. The black line is the cumulative total modeled evapotranspiration (ET) for P300 and the dashed green line is the total calculated ET using measured latent heat (LH) from the P301 eddy covariance flux tower.

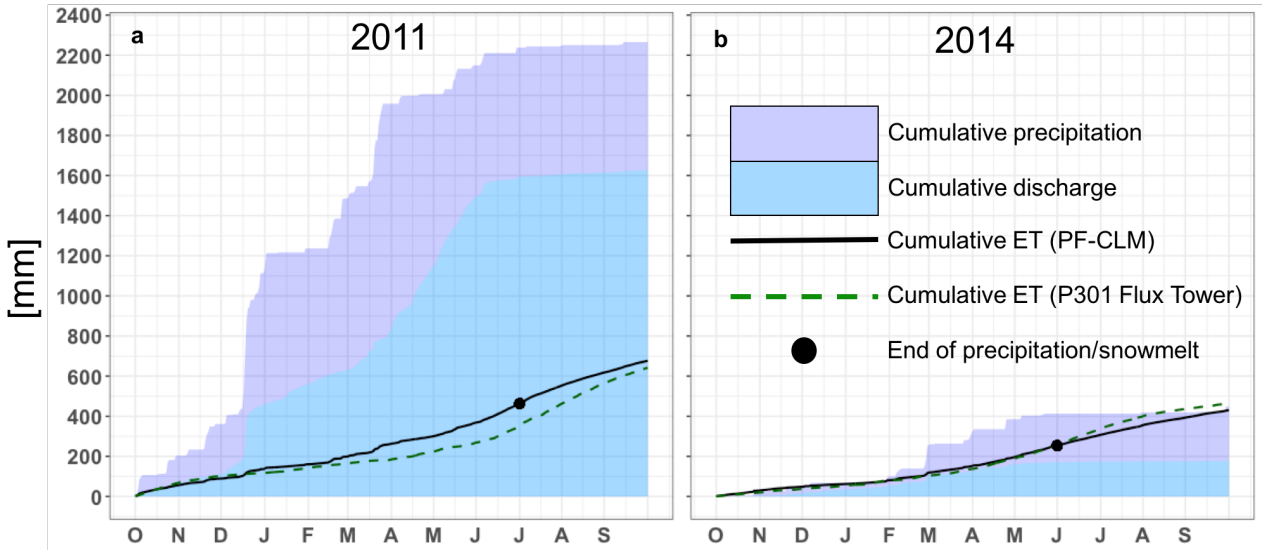


Figure 3.2 Annual P300 water balance: (a) 2011, a pre-drought year; (b) 2014, after sustained drought. Purple shading depicts cumulative precipitation, blue shading depicts cumulative discharge, solid black line depicts cumulative modeled evapotranspiration (ET), dashed green line depicts cumulative observed ET, and black dot depicts the end of precipitation and snowmelt.

Total evapotranspiration (ET) estimates from the P301 tower are 642 mm for 2011 and 463 mm for 2014. These estimates compare well to the total modeled ET for the base case simulation of 677 mm for 2011 and 431 mm for 2014. However, the major assumption is that P301 flux tower ET footprint is representative of all of P300. Total evapotranspiration exceeds total precipitation during the drought period years suggesting vegetation is sustained by plant-accessible groundwater storage (Figures 3.1 and 3.2B). This finding is consistent with recent research (Bales et al. 2018).

3.2 Critical Zone Relationships with Water Table Depth

PF-CLM is a tool for studying evapotranspiration (ET) components separately. The conceptual model in Figure 3.3A explores evapotranspiration component behavior in an ideal hillslope where transpiration and evaporation are not water limited in shallow water table depths (convergence zones) and shut off in water limited areas where deeper water tables exist (ridges) (Maxwell and Condon 2016). As water table depth increases, evaporation shuts off in energy and water limited ridges before transpiration but is maintained through the drought by lateral groundwater flow into convergence zones.

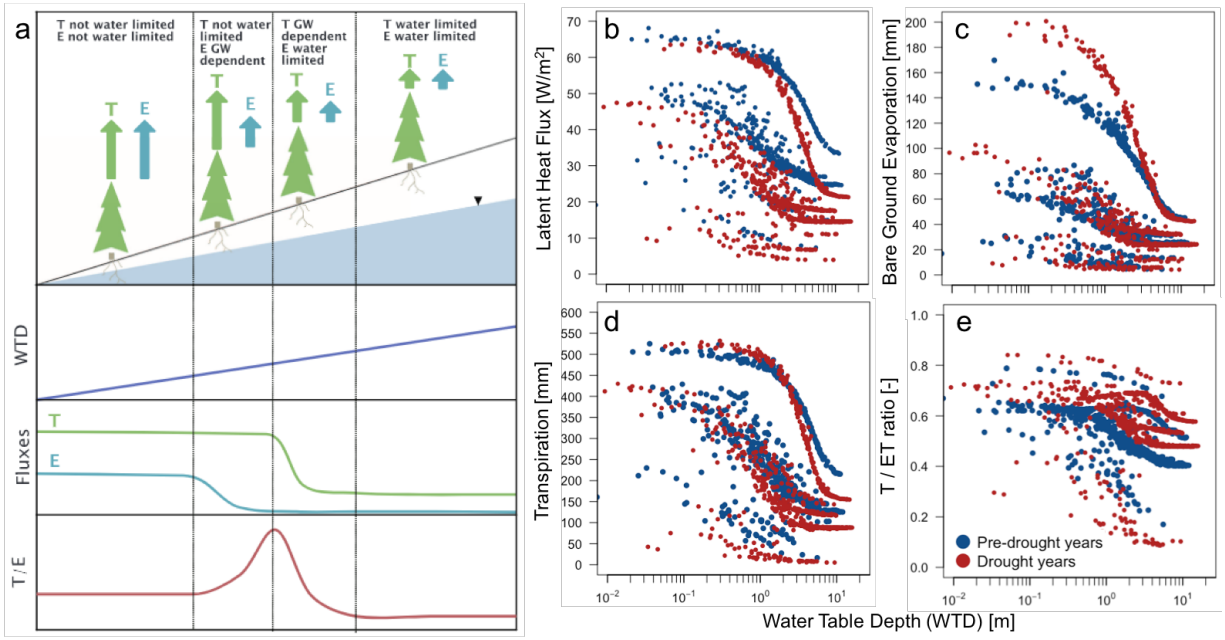


Figure 3.3 Evapotranspiration (ET) relationships with water table depth (WTD): (a) Maxwell and Condon conceptual model (2016); (b) latent heat flux relationship with WTD; (c) bare ground evaporation relationship with WTD; (d) transpiration relationship with WTD; (e) transpiration partitioning ratio (T/ET) relationship with WTD. Each blue symbol depicts the average total ET component for one cell over the pre-drought period and each red symbol depicts the average total ET component for one cell over the drought period.

Figure 3.3B-E explores how these ET-WTD relationships evolved during the recent California Drought at P300. Blue and red symbols represent the average ET component during the pre-drought and drought years, respectively. During the drought period, increases in energy input with increasing air temperature cause bare ground

evaporation to become more sensitive to changes in water table (Figure 3.3C). During the drought, bare ground evaporation increases significantly in the non-water limited convergence zones (shallow water table depths) and shuts off in the already energy-limited ridges (deeper water table depths) (Figure 3.3C). Transpiration sensitivity to changes in water table also increases during the drought (Figure 3.3D). During drought conditions, transpiration in the non-water limited convergence zones is maintained. Despite significant decreases in precipitation during the drought, transpiration dominates the evapotranspiration (ET) balance (Figure 3.3E).

3.3 Evapotranspiration through the recent California Drought

The evapotranspiration (ET) estimates discussed in Figure 3.3 can be visualized spatially (Figures 3.4 and A-3). Figure 3.4 depicts the total annual evapotranspiration (ET), total annual bare ground evaporation (E), total annual transpiration (T), and the total annual transpiration partitioning ratio (T/ET) in Providence Creek watershed (P300) for the base case model simulation. Decreases in ET components are most pronounced in the ridges where deeper water table depths (WTDs) are prevalent and sustained in the convergence zones where shallower WTDs are both non-water and non-energy limited. The spatial extent of T/ET decreases in the ridges where WTD increases and plant-accessible groundwater diminishes. Lateral groundwater flow sustains transpiration in the convergence zones.

For the base case, total evapotranspiration for P300 decreased by 26.5% from an annual average of 615 mm during the pre-drought period to 452 mm annual average during the drought period. The total bare ground evaporation (E) in P300 decreased by 1.1% from an annual average of 94 mm during the pre-drought period to 93 mm annual average during the drought period. The total transpiration (T) for P300 decreased by 20.9% from an annual average of 363 mm during the pre-drought period to 287 mm annual average during the drought period. Total precipitation (P) in P300 decreased by 68.8% from an annual average of 1706 mm during the pre-drought period to 652 mm annual average during the drought period. Total stream discharge at the P300 outlet decreases by 71.5% from an annual average of 1139 mm during the pre-drought period to 325 mm annual average during the drought period. Total annual average change in

storage for P300 during the pre-drought period was 23 mm. This increase in total change in storage is attributed to the 38% increase in precipitation from water year 2010 to water year 2011. Total annual average change in storage for P300 during the drought period decreased by 85 mm.

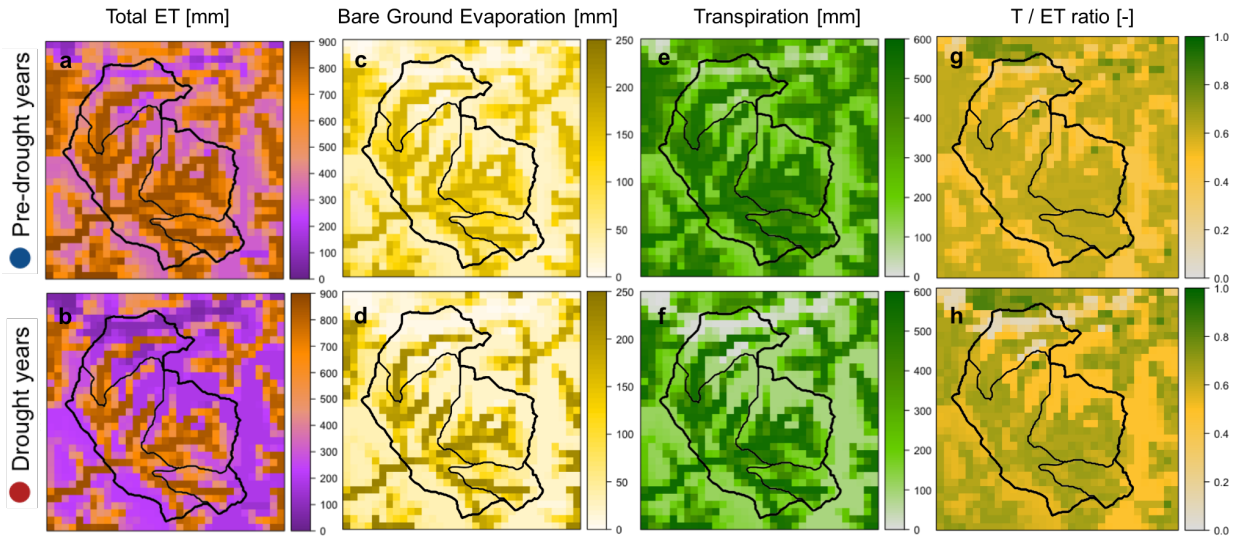


Figure 3.4 Visualizing evapotranspiration spatially for the base case model: (a-b) total evapotranspiration averaged over the pre-drought period (a) and the drought period (b); (c-d) total bare ground evaporation averaged over the pre-drought period (c) and the drought period (d); (e-d) total transpiration averaged over the pre-drought period (e) and the drought period (f); (g-h) total transpiration partitioning ratio averaged over the pre-drought period (cg and the drought period (h).

Similar to Figure 3.4, Figure A-3 depicts the spatial variation in the evapotranspiration (ET) components and the transpiration partitioning ratio (T/ET) for each of the model variations in Figure A-2, including the free-draining model.

For the double permeability case, total evapotranspiration (ET) decreased by 21.6% from an annual average of 529 mm during the pre-drought period to 415 mm annual average during the drought period. Total bare ground evaporation (E) increased by 8.7% from an annual average of 79 mm during the pre-drought period to 86 mm annual average during the drought period. Total transpiration (T) decreased by 11.9% from an annual average 293 mm during the pre-drought period to 258 mm annual average during the drought period. Total stream discharge at the P300 outlet decreases by 67.3% from an annual average of 1170 mm during the pre-drought period to 383 mm

annual average during the drought period. Total annual average change in storage decreases by 245.9% from 74 mm annual average during the pre-drought period to -108 mm annual average during the drought period. The transpiration partitioning ratio (T/ET) increases from 55.4% during the pre-drought period to 62.2% during the drought period.

Water Balance Component	Model	Pre-Drought Years					Drought Years				
		P300	P301	P303	P304	Domain	P300	P301	P303	P304	Domain
Precipitation [mm]	NLDAS-II Precip	1706	1718	1713	1695	1706	652	657	652	647	653
Bare Ground Evaporation [mm]	Base Case	94	81	94	106	80	93	80	92	102	77
	Free-draining Case	33	23	35	42	29	32	22	33	39	28
	Homogeneous Geology Case	95	82	95	107	81	92	79	92	101	76
	Double Permeability Case	79	66	77	85	66	86	71	82	88	70
	Quadruple Permeability Case	67	54	62	68	56	73	62	64	73	59
Transpiration [mm]	Base Case	363	324	361	407	335	287	245	288	316	257
	Free-draining Case	157	112	167	192	140	115	77	121	142	103
	Homogeneous Geology Case	366	326	364	411	337	285	243	285	313	254
	Double Permeability Case	293	255	284	322	267	258	207	247	270	224
	Quadruple Permeability Case	248	199	234	260	220	211	170	186	210	179
Total Evapotranspiration [mm]	Base Case	615	561	613	672	568	452	396	452	490	403
	Free-draining Case	350	293	359	392	323	218	169	224	252	200
	Homogeneous Geology Case	619	564	616	677	571	449	394	449	486	401
	Double Permeability Case	529	477	517	565	486	415	349	401	431	364
	Quadruple Permeability Case	474	411	455	488	429	355	303	321	353	307
Discharge [mm]	Base Case	1139	77	1026	1581	536	325	13	282	443	157
	Free-draining Case	NA	NA	NA	NA	NA	NA	NA	NA	NA	NA
	Homogeneous Geology Case	1141	77	1030	1589	537	426	21	374	586	203
	Double Permeability Case	1170	74	1013	1617	559	383	13	345	501	187
	Quadruple Permeability Case	1124	53	952	1390	549	480	9	433	511	246
Runoff Ratio [-]	Base Case	0.65	0.04	0.59	0.91	0.31	0.49	0.02	0.43	0.67	0.24
	Free-draining Case	0.00	0.00	0.00	0.00	0.00	0.00	0.00	0.00	0.00	0.00
	Homogeneous Geology Case	0.66	0.04	0.59	0.92	0.31	0.69	0.03	0.61	0.96	0.33
	Double Permeability Case	0.67	0.04	0.58	0.94	0.32	0.59	0.02	0.54	0.78	0.29
	Quadruple Permeability Case	0.65	0.03	0.55	0.80	0.32	0.76	0.01	0.69	0.80	0.39
Δ Storage [mm]	Base Case	23	21	46	37	16	-85	-66	-113	-98	-78
	Free-draining Case	978	945	941	987	985	-334	-346	-337	-326	-336
	Homogeneous Geology Case	19	19	39	28	11	-71	-52	-92	-81	-64
	Double Permeability Case	74	59	122	99	64	-108	-94	-141	-127	-102
	Quadruple Permeability Case	138	131	163	167	143	-152	-136	-181	-162	-158

Table 3.1 Total Annual Evapotranspiration (ET) Components, Water Balance Components, and Runoff Ratios for Pre-drought and Drought Periods. Values are averaged for pre-drought years (2009-2011) and drought years (2012-2016).

For the quadruple permeability case, total evapotranspiration (ET) decreased by 25.1% from an annual average of 474 mm during the pre-drought period to 355 mm annual average during the drought period. Total bare ground evaporation (E) increased by 9.0% from an annual average of 67 mm during the pre-drought period to 73 mm annual average during the drought period. Total transpiration (T) decreased by 14.9% from an annual average 248 mm during the pre-drought period to 211 mm annual average during the drought period. Total stream discharge at the P300 outlet decreases

by 57.3% from an annual average of 1124 mm during the pre-drought period to 480 mm annual average during the drought period. Total annual average change in storage decreases by 210.1% from 138 mm annual average during the pre-drought period to -152 mm annual average during the drought period. The transpiration partitioning ratio (T/ET) increases from 52.3% during the pre-drought period to 59.4% during the drought period.

For the free-draining model, without lateral groundwater flow, ET is controlled by soil and geology and decreases ubiquitously across the watershed. Total evapotranspiration (ET) decreases by 37.7% from an annual average of 350 mm during the pre-drought period to 218 mm annual average during the drought period. Total bare ground evaporation (E) decreases by 3.0% from an annual average of 33 mm during the pre-drought period to 32 mm annual average during the drought period. Total transpiration (T) decreases by 26.8% from an annual average of 157 mm during the pre-drought period to 115 mm annual average during the drought.

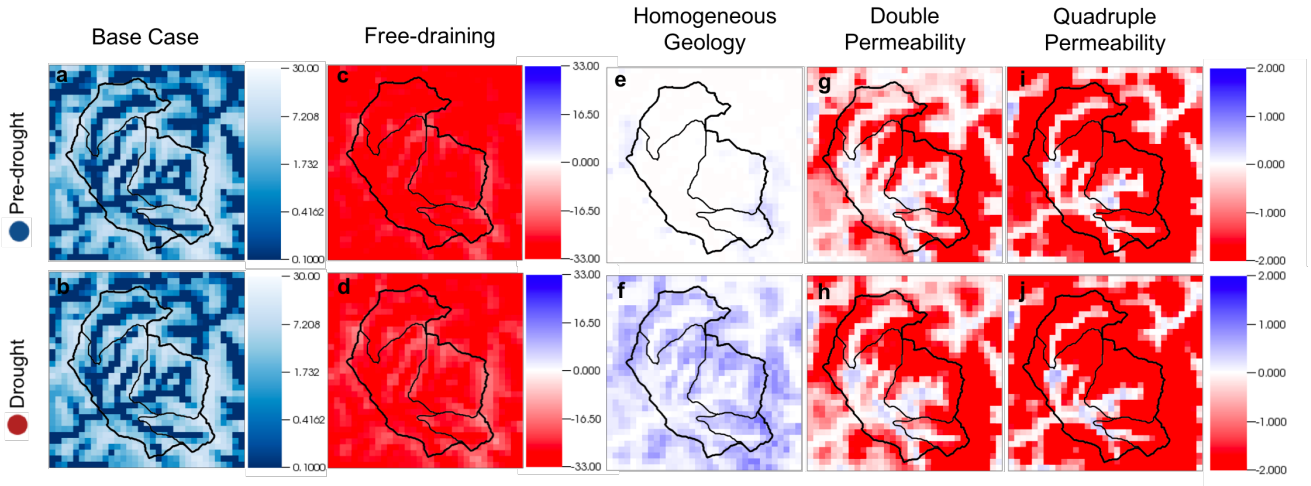


Figure 3.5 The sensitivity of water table depth (WTD) to subsurface characterization: (a-b) base case model; (c-d) difference between base case model and free-draining model; (e-f) difference between base case model and homogenous geology model; (g-h) difference between base case model and double permeability model; (i-j) difference between base case model and quadruple permeability model. For panels a-b, the dark blue indicates shallower WTDs whereas light blue indicates deeper WTDs. Panels c-j show the different in WTD for the pre-drought and drought periods for the four additional subsurface characterizations from the base case model. Blue indicates more water than base case model and red indicates less water than base case model.

Figure A-4 shows the total annual average water table depth (WTD) for the pre-drought and drought periods (a-j) and how the WTD changes during the drought (k-o) for all model characterizations, where dark blue indicates more water/shallower water table depths (WTDs) and light blue indicates less water/deeper water table depths (WTDs). The blue in the difference plots in Figure 3.5 indicates more water in the model than the base case and red indicates less water than the base case. Figure 3.5 shows the total annual average water table depth (WTD) for the pre-drought and drought periods for the base case model (a-b) and the difference between the total annual WTD of the base case model and the four additional model characterizations (c-j). Decreasing effective domain permeability produces increases in WTD (e-f) whereas increasing effective domain permeability produced decreases in WTD (g-j). By design, the free-draining model effectively removes groundwater producing significant decreases in WTD from the base case (c-d).

For the homogeneous geology, double, and quadruple permeability cases the spatial variation in how ET occurs at Providence Creek (P300) is similar to the base case: ET decreases in the ridges and increases in the convergence zones. Similar to the heterogeneous models, the transpiration partitioning ratio (T/ET) for the free-draining model (Figure A-4) increases from 44.9% during the pre-drought period to 52.8% during the drought period. The increase in transpiration partitioning across models is due to total evapotranspiration (ET) decreasing more than transpiration (T). Despite the difference in the subsurface characterizations, ET behavior remains the same for each model into the drought period. Increasing the overall effective domain permeability reduces water table depths—a proxy for how extensive plant-accessible groundwater is. Despite slight reductions in overall evapotranspiration (ET) through the drought, lateral groundwater flow maintains transpiration preventing total shut off and subsequent die off.

3.4 Lateral Groundwater Flow on Transpiration through the California Drought

The total transpiration partitioning ratio (T/ET) for P300 increased from an annual average of 59.0% during the pre-drought period to 63.5% annual average during the drought period.

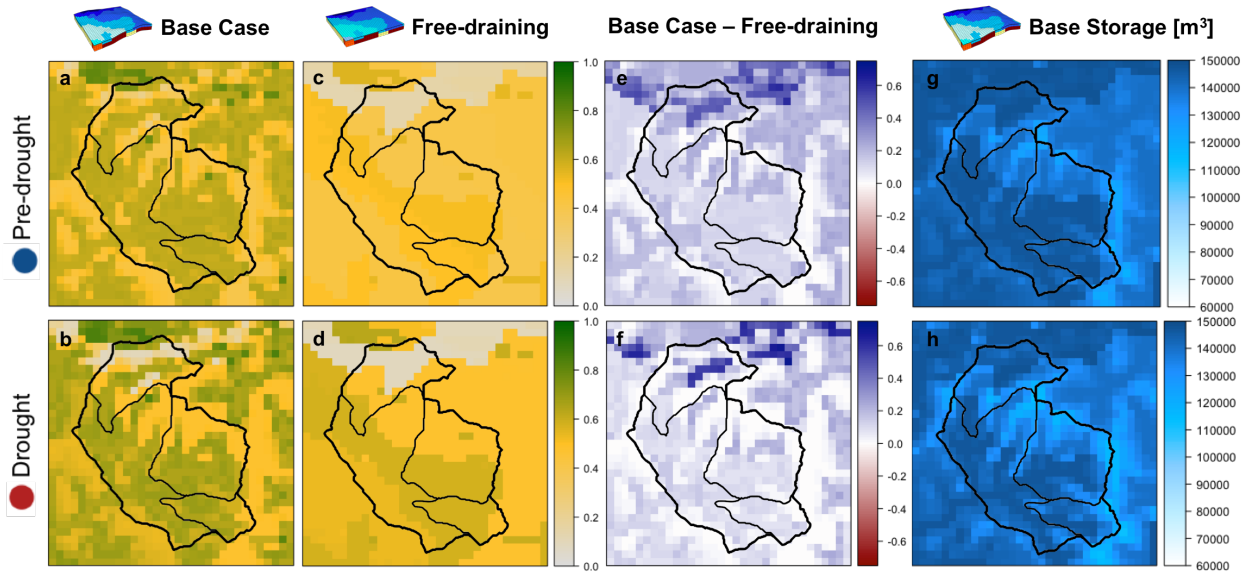


Figure 3.6 The effect of lateral groundwater flow on transpiration partitioning (T/ET): (a-b) T/ET for base case model; (c-d) T/ET for free-draining model; (e-f) the difference in T/ET for base case model and free-draining model; (g-h) base case groundwater storage.

From the pre-drought period to the drought period the change in groundwater storage decreased by 470% sustaining evapotranspiration. Despite the 68.8% decrease in precipitation during the drought years, ET only decreases 26.5% during the drought period. Evapotranspiration is essentially maintained at P300 during the drought period: 463 mm in 2012, 457 mm in 2013, 431 mm in 2014, 424 mm in 2015, and 484 mm in 2016. There is not a surplus of precipitation into the system during the drought period to account for the evapotranspiration flux and discharge out of the system. The additional outgoing flux—through discharge and evapotranspiration—is sourced from groundwater storage.

For the pre-drought and drought periods, Figure 3.6 depicts the transpiration partitioning (T/ET) ratio for the base case model (Figure 3.6A-B) and the free-draining model (Figure 3.6C-D). Transpiration in the base case model is sustained due to lateral groundwater flow. In the free-draining model, groundwater is effectively removed from the system and transpiration is controlled by soil and geology. Figure 3.6E-F shows the transpiration partitioning ratio (T/ET) of the free-draining model removed from that of the base case effectively showing the fraction of groundwater being transpired. The spatial

pattern that emerges in Figure 3.6E-F closely resembles the base case groundwater storage (Figure 3.6G-H) suggesting transpiration is sourcing groundwater storage.

CHAPTER 4
CONCLUSIONS

Urban and agricultural water use is directly sourced from mountain headwaters. Accurate and comprehensive water budget knowledge is imperative especially in regions, such as California, where prolonged drought periods are becoming more frequent under changing climate regimes (Fulé et al. 2012; Westerling et al. 2006). As the largest terrestrial flux, it is critical to bracket evapotranspiration (ET) estimates (Trenberth et al. 2007).

Evapotranspiration is difficult to estimate in the field. In many mountain regions experiencing sustained drought, expansive and increasing tree-mortality is observed. During the recent California Drought, tree mortality in the Southern Sierras has broadened and encroached into the Providence Creek watershed (P300) (Bales et al. 2018). Recent research suggests that plants are using more water than originally thought (Maxwell and Condon 2016). In this study, an integrated modeling approach is used to bridge the gap between point-observations and the spatial complexity of evapotranspiration (ET) and to explore the role of lateral groundwater flow on the drought-tolerance of P300 vegetation.

Despite a significant decrease in precipitation during the drought period, evapotranspiration at P300 is maintained. From the pre-drought period to the drought period the total change in groundwater storage decreased by 470%. Groundwater storage helps explain how P300 vegetation sustained through the drought. Incorporating lateral groundwater flow increased transpiration partitioning (T/ET) from 44.9% to 59.0% in the pre-drought period and from 52.8% to 63.5% in the drought period. These model simulations strongly suggest that lateral groundwater flow sustained P300 vegetation and ET fluxes through the drought.

Integrated, physically-based models provide an avenue for exploring evapotranspiration partitioning mechanistically. These tools help to bridge the gap between point observations and the spatial complexity of hydrologic fluxes. Bracketing these fluxes is sensitive to subsurface characterization. Understanding subsurface heterogeneities in mountain systems is challenging and demands extensive observation. These experiments can inform data collection. However, hydrology

modeling is not without caveats. Limitations of the model include uncertainty within the model parameters—hydraulic conductivity, porosity, land cover, to name a few—and model design—lateral and vertical resolution. Further increasing the degree of heterogeneity and increasing the resolution would help to resolve system behavior. Nevertheless, these computational experiments add to the body of evidence supporting lateral groundwater flow as a mechanism for plant water use during drought stress.

REFERENCES CITED

Ashby, S. F., and R. D. Falgout. 1996. “A Parallel Multigrid Preconditioned Conjugate Gradient Algorithm for Groundwater Flow Simulations.” *Nuclear Science and Engineering* 124 (1): 145–59. http://www.ans.org/pubs/journals/nse/a_24230.

Bales, R., M. Conklin, M. Hart, A. A. Berhe, A. T. O’Geen, S. Glaser, C. Tague, et al. 2014. “Southern Sierra CZO and Kings River Experimental Watershed (KREW).”

Bales, Roger C., Michael L. Goulden, Carolyn T. Hunsaker, Martha H. Conklin, Peter C. Hartsough, Anthony T. O’Geen, Jan W. Hopmans, and Mohammad Safeeq. 2018. “Mechanisms Controlling the Impact of Multi-Year Drought on Mountain Hydrology.” *Scientific Reports* 8 (1): 1–8. doi:10.1038/s41598-017-19007-0.

Bateman, Paul Charles, and David R Wones. 1972. “Geologic Map of the Huntington Lake Quadrangle, Central Sierra Nevada, California.” *United States Geologic Survey Geologic Quadrangle Map*. Washington, D.C. http://pubs.er.usgs.gov/publication/gq987.

Beniston, Martin. 2003. “Climatic Change in Mountain Regions: A Review of Possible Impacts.” *Climatic Change* 59 (1): 5–31. doi:10.1023/A:1024458411589.

Beniston, Martin, Douglas G. Fox, S. Adhikary, R. Andressen, A. Guisan, J. I. Holten, J. Innes, et al. 1996. “Impacts of Climate Change on Mountain Regions.” Edited by Robert T. Watson, M. C. Zinyowera, and Richard H. Moss. *Climate Change 1995: The IPCC Second Assessment Report*. Cambridge: Cambridge University Press. https://publications.csiro.au/rpr/pub?list=BRO&pid=procite:e13d5eca-5ed6-4e2d-a9a7-e360752e3c51.

Blankinship, Joseph C., Matthew W. Meadows, Ryan G. Lucas, and Stephen C. Hart. 2014. “Snowmelt Timing Alters Shallow but Not Deep Soil Moisture in the Sierr.” *Water Resources Research*, 1448–56. doi:10.1002/2013WR014222.Received.

Condon, Laura E., Reed M. Maxwell, and Subhrendu Gangopadhyay. 2013. “The Impact of Subsurface Conceptualization on Land Energy Fluxes.” *Advances in Water Resources* 60. Elsevier Ltd: 188–203. doi:10.1016/j.advwatres.2013.08.001.

Cosgrove, Brian A., Dag Lohmann, Kenneth E. Mitchell, Paul R. Houser, Eric F. Wood, John C. Schaake, Alan Robock, et al. 2003. “Real-Time and Retrospective Forcing in the North American Land Data Assimilation System (NLDAS) Project.” *Journal of Geophysical Research* 108 (D22): 8842. doi:10.1029/2002JD003118.

Dai, Yongjiu, Xubin Zeng, Robert E. Dickinson, Ian Baker, Gordon B. Bonan, Michael G. Bosilovich, A. Scott Denning, et al. 2003. “The Common Land Model.” *Bulletin of the American Meteorological Society* 84 (8): 1013–23. doi:10.1175/BAMS-84-8-1013.

Ferguson, Ian M., Jennifer L. Jefferson, Reed M. Maxwell, and Stefan J. Kollet. 2016. "Effects of Root Water Uptake Formulation on Simulated Water and Energy Budgets at Local and Basin Scales." *Environmental Earth Sciences* 75 (4). Springer Berlin Heidelberg: 1–15. doi:10.1007/s12665-015-5041-z.

Fulé, Peter Z., Joseph E. Crouse, John Paul Roccaforte, and Elizabeth L. Kalies. 2012. "Do Thinning And/or Burning Treatments in Western USA Ponderosa or Jeffrey Pine-Dominated Forests Help Restore Natural Fire Behavior?" *Forest Ecology and Management* 269 (2012): 68–81. doi:10.1016/j.foreco.2011.12.025.

Graham, R C, K R Tice, and W R Guertal. 1994. "The Pedologic Nature of Weathered Rock." In *Whole Regolith Pedology*, edited by David L. Cremeens, Randall Barber Brown, and James Herbert Huddleston, 21–40. Soil Science Socoety of America.

Holbrook, W. Steven, Clifford S. Riebe, Mehrez Elwaseif, Jorden L. Hayes, Kyle Basler-Reeder, Dennis L. Harry, Armen Malazian, Anthony Dosseto, Peter C. Hartsough, and Jan W. Hopmans. 2014. "Geophysical Constraints on Deep Weathering and Water Storage Potential in the Southern Sierra Critical Zone Observatory." *Earth Surface Processes and Landforms* 39 (3): 366–80. doi:10.1002/esp.3502.

Homer, C.G., J.A. Dewitz, L. Yang, S. Jin, P. Danielson, G. Xian, J. Coulston, N.D. Herold, J.D. Wickham, and 2015 Megown, K. 2015. "Completion of the 2011 National Land Cover Database for the Conterminous United States-Representing a Decade of Land Cover Change Information." *Photogrammetric Engineering and Remote Sensing* 8 (5): 345–54.

Hubbert, K R, R C Graham, and M A Anderson. 2001. "Soil and Weathered Bedrock: Components of a Jeffrey Pine Plantation Substrate." *Soil Science Society of America Journal* 65 (4): 1255–62.

IPCC. 2014. "Summary for Policymakers." *Climate Change 2014: Synthesis Report. Contribution of Working Groups I, II and III to the Fifth Assessment Report of the Intergovernmental Panel on Climate Change*. doi:10.1017/CBO9781107415324.

Jefferson, Jennifer L., James M. Gilbert, Paul G. Constantine, and Reed M. Maxwell. 2015. "Active Subspaces for Sensitivity Analysis and Dimension Reduction of an Integrated Hydrologic Model." *Computers & Geosciences* 83 (October): 127–38. doi:10.1016/j.cageo.2015.07.001.

Jefferson, Jennifer L., and Reed M. Maxwell. 2015. "Evaluation of Simple to Complex Parameterizations of Bare Ground Evaporation." *Journal of Advances in Modeling Earth Systems* 7 (3): 1075–92. doi:10.1002/2014MS000398.

Jepsen, S.M., T.C. Harmon, M.W. Meadows, and C.T. Hunsaker. 2016. "Hydrogeologic Influence on Changes in Snowmelt Runoff with Climate Warming: Numerical

Experiments on a Mid-Elevation Catchment in the Sierra Nevada, USA." *Journal of Hydrology* 533 (February 2016): 332–42. doi:10.1016/j.jhydrol.2015.12.010.

Jones, Jim E., and Carol S. Woodward. 2001. "Newton-Krylov-Multigrid Solvers for Large-Scale, Highly Heterogeneous, Variably Saturated Flow Problems." *Advances in Water Resources* 24: 763–74. doi:10.1016/S0309-1708(00)00075-0.

Kelly, Anne E., and Michael L. Goulden. 2016. "A Montane Mediterranean Climate Supports Year-Round Photosynthesis and High Forest Biomass." *Tree Physiology* 36 (4): 459–68. doi:10.1093/treephys/tpv131.

Kollet, Stefan J., and Reed M. Maxwell. 2006. "Integrated Surface–groundwater Flow Modeling: A Free-Surface Overland Flow Boundary Condition in a Parallel Groundwater Flow Model." *Advances in Water Resources* 29 (7): 945–58. doi:10.1016/j.advwatres.2005.08.006.

———. 2008a. "Capturing the Influence of Groundwater Dynamics on Land Surface Processes Using an Integrated, Distributed Watershed Model." *Water Resources Research* 44 (2): 1–18. doi:10.1029/2007WR006004.

———. 2008b. "Capturing the Influence of Groundwater Dynamics on Land Surface Processes Using an Integrated, Distributed Watershed Model." *Water Resources Research* 44 (2): n/a-n/a. doi:10.1029/2007WR006004.

Kollet, Stefan J., Reed M. Maxwell, Carol S. Woodward, Steve Smith, Jan Vanderborght, Harry Vereecken, and Clemens Simmer. 2010. "Proof of Concept of Regional Scale Hydrologic Simulations at Hydrologic Resolution Utilizing Massively Parallel Computer Resources." *Water Resources Research* 46 (4): 1–7. doi:10.1029/2009WR008730.

Liu, Fengjing, Carolyn Hunsaker, and Roger C. Bales. 2013. "Controls of Streamflow Generation in Small Catchments across the Snow-Rain Transition in the Southern Sierra Nevada, California." *Hydrological Processes* 27 (14): 1959–72. doi:10.1002/hyp.9304.

Maxwell, Reed M. 2013. "A Terrain-Following Grid Transform and Preconditioner for Parallel, Large-Scale, Integrated Hydrologic Modeling." *Advances in Water Resources* 53: 109–17. doi:10.1016/j.advwatres.2012.10.001.

Maxwell, Reed M., and Stefan J. Kollet. 2008. "Interdependence of Groundwater Dynamics and Land-Energy Feedbacks under Climate Change." *Nature Geoscience* 1: 665–69. doi:10.1038/ngeo315.

Maxwell, Reed M., and Norman L. Miller. 2005. "Development of a Coupled Land Surface and Groundwater Model." *Journal of Hydrometeorology* 6 (3): 233–47. doi:10.1175/JHM422.1.

Maxwell, Reed M, and Laura E Condon. 2016. “Connections between Groundwater Flow and Transpiration Partitioning.” *Science* 353 (6297): 377–80. doi:10.1126/science.aaf7891.

Mitchell, Kenneth E, Dag Lohmann, Paul R Houser, Eric F Wood, John C Schaake, Alan Robock, Brian a Cosgrove, et al. 2004. “The Multi-Institution North American Land Data Assimilation System (NLDAS): Utilizing Multiple GCIP Products and Partners in a Continental Distributed Hydrological Modeling System.” *J. Geophys. Res.* 109 (D7): D07S90--. doi:10.1029/2003JD003823.

National Science Foundation. 2016a. “Critical Zone Observatories: U.S. NSF National Program.” http://criticalzone.org/national/about/.

———. 2016b. “Infrastructure.” http://criticalzone.org/national/research/the-critical-zone-1national/.

———. 2016c. “Southern Sierra Critical Zone Observatory: About.” http://criticalzone.org/sierra/about/.

Osei-Kuffuor, D., R. M. Maxwell, and C. S. Woodward. 2014. “Improved Numerical Solvers for Implicit Coupling of Subsurface and Overland Flow.” *Advances in Water Resources* 74. Elsevier Ltd: 185–95. doi:10.1016/j.advwatres.2014.09.006.

Safeeq, Mohammad, and Carolyn T. Hunsaker. 2016. “Characterizing Runoff and Water Yield for Headwater Catchments in the Southern Sierra Nevada.” *JAWRA Journal of the American Water Resources Association* 93710. doi:10.1111/1752-1688.12457.

Soil Survey Staff, Natural Resources Conservation Service, United States Department of Agriculture. 2017. “Web Soil Survey.” https://websoilsurvey.sc.egov.usda.gov/.

Southern Sierra Critical Zone Observatory. 2016. “Providence Creek Headwater Catchments: Climate.” http://criticalzone.org/sierra/infrastructure/field-area/providence-creek-headwaters/.

Tague, Christina, and Aubrey L. Dugger. 2010. “Ecohydrology and Climate Change in the Mountains of the Western USA - A Review of Research and Opportunities.” *Geography Compass* 4 (11): 1648–63. doi:10.1111/j.1749-8198.2010.00400.x.

Trenberth, K E, L Smith, T T Qian, A Dai, and J Fasullo. 2007. “Estimates of the Global Water Budget and Its Annual Cycle Using Observational and Model Data.” *Journal of Hydrometeorology* 8 (4): 758–69. doi:10.1175/jhm600.1.

U.S. Geological Survey. 2017. “2012-2016 California Drought: Historical Perspective.” https://ca.water.usgs.gov/california-drought/california-drought-comparisons.html.

Westerling, A. L., H. G. Hidalgo, D. R. Cayan, and T. W. Swetnam. 2006. “Warming and Earlier Spring Increase Western U.S. Forest Wildfire Activity.” *Science* 313 (5789): 940–43. doi:10.1126/science.1128834.

APPENDIX

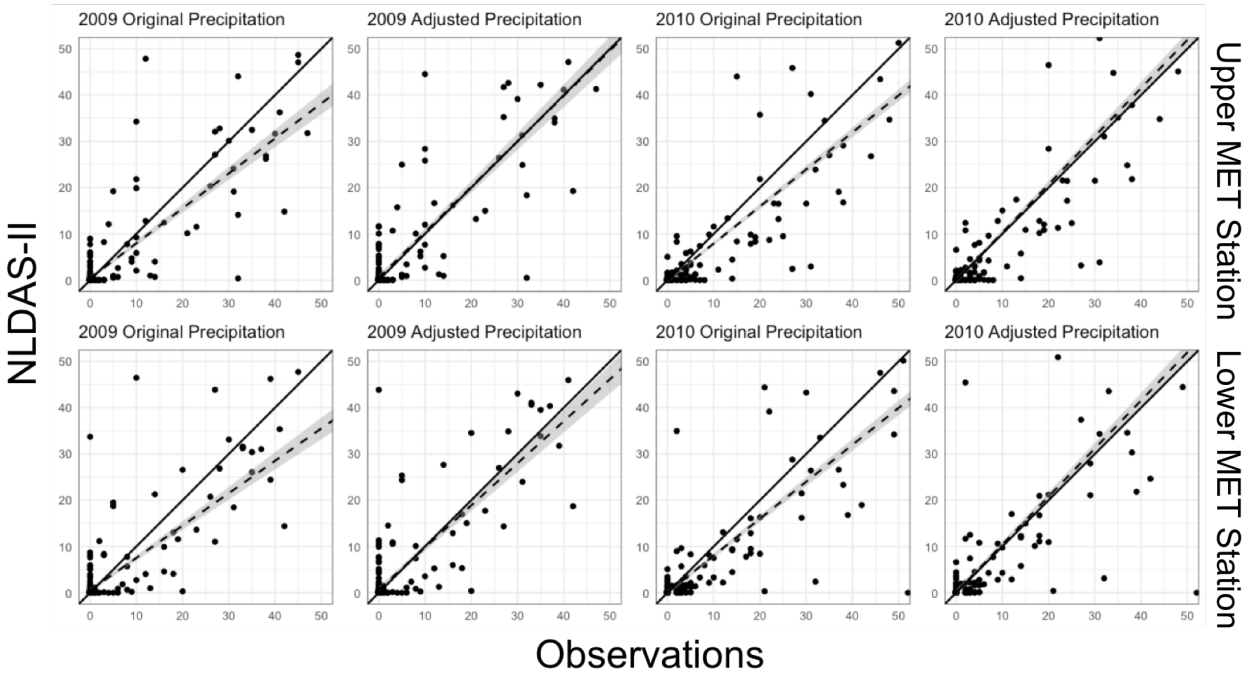


Figure A.1 Original and adjusted NLDAS-II precipitation. Dashed line shows the relationship between NLDAS-II values and observations from the upper MET station (first row) and lower MET station (second row). Solid line is the 1:1 ratio.

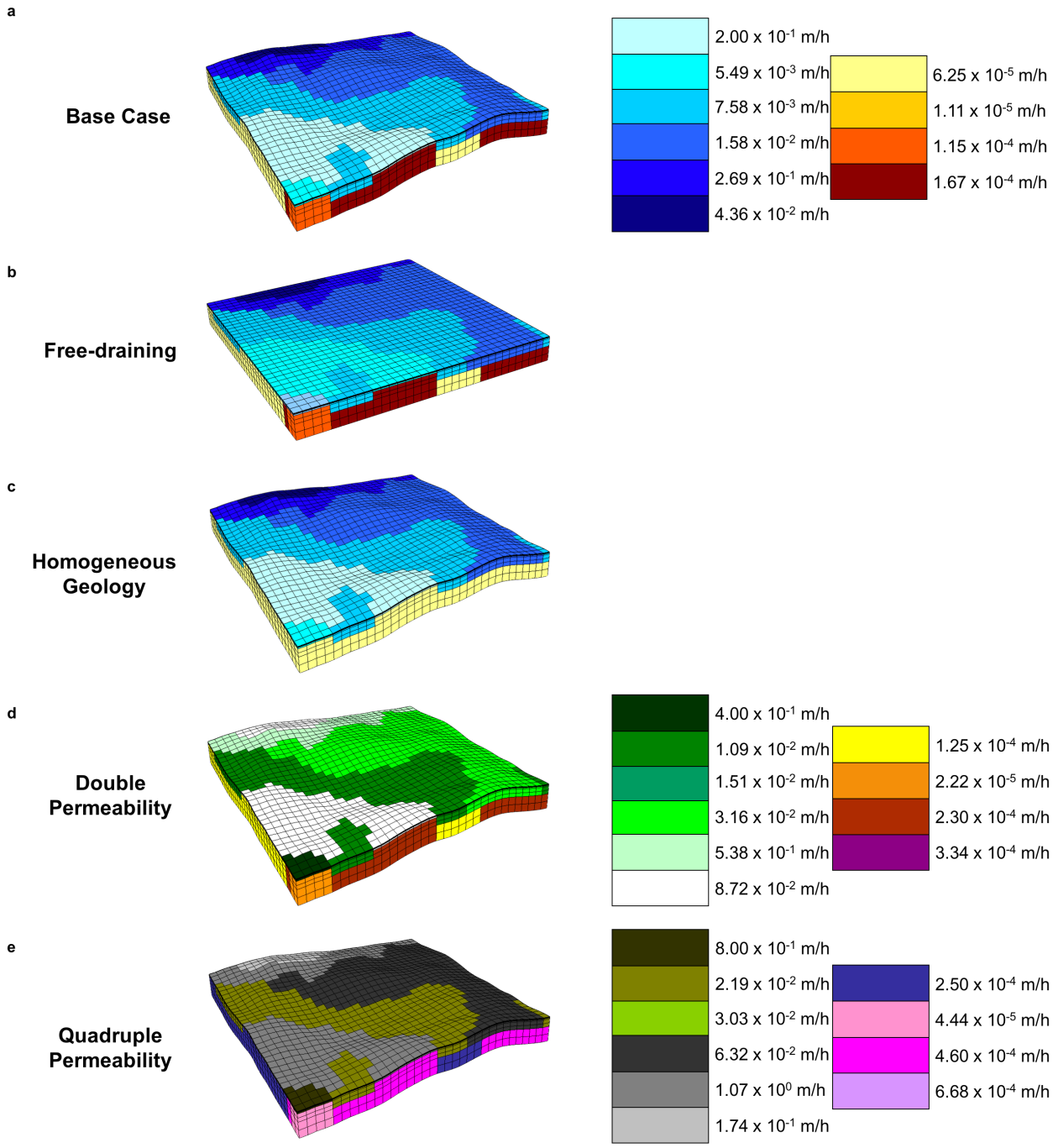


Figure A.2 Visualizing the subsurface sensitivity study: (a) base case model; (b) free-draining model; (c) homogeneous geology model; (d) double permeability model; (e) quadruple permeability model.

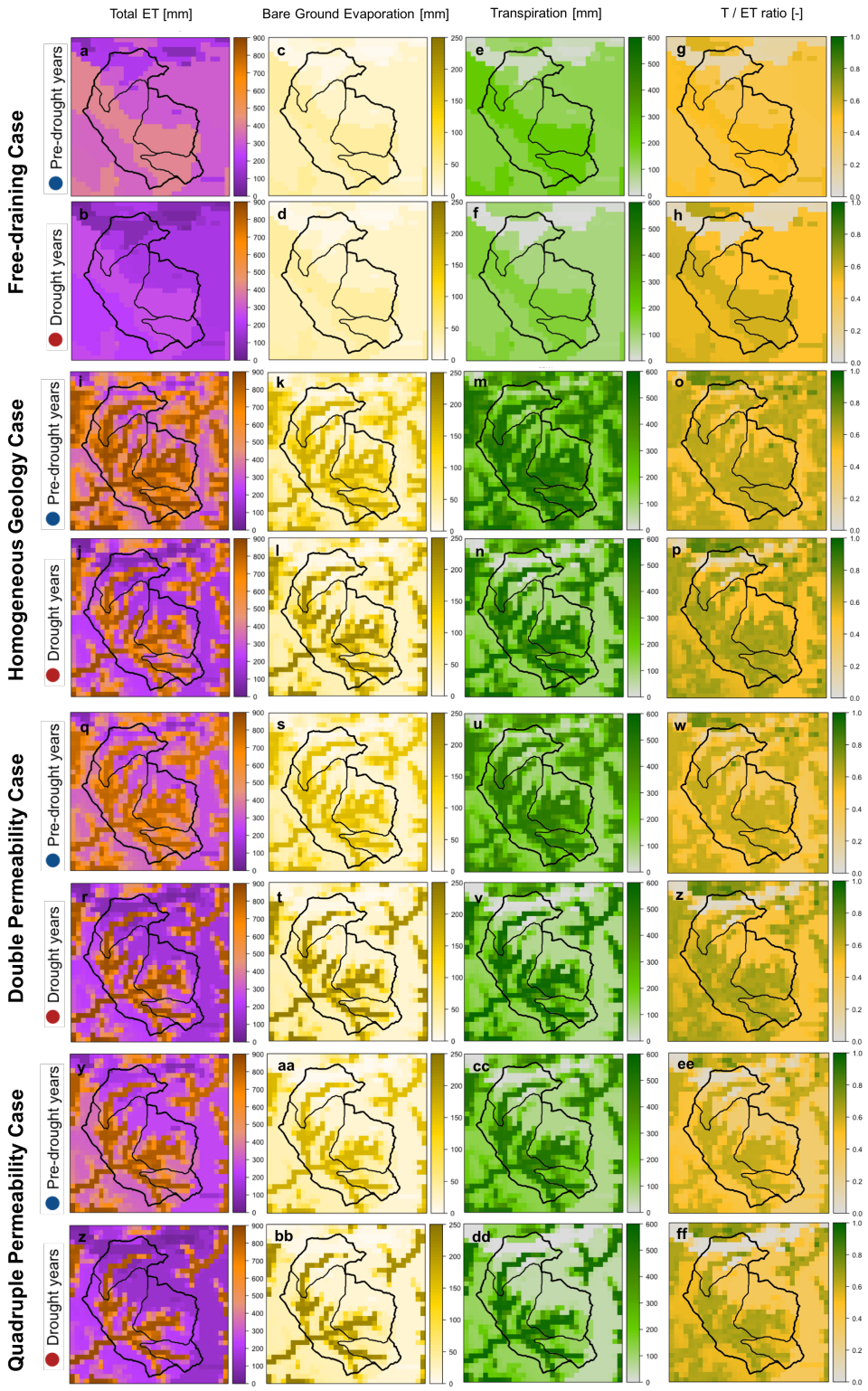


Figure A.3 Visualizing evapotranspiration spatially for subsurface sensitivity study: total evapotranspiration averaged over the pre-drought period and the drought period for the free-draining model (a-b), homogeneous geology model (i-j), double permeability model (q-r), and quadruple permeability model (y-z); total bare ground evaporation

averaged over the pre-drought period and the drought period for the free-draining model (c-d), homogeneous geology model (k-l), double permeability model (s-t), and quadruple permeability model (aa-bb); total transpiration averaged over the pre-drought period and the drought period for the free-draining model (e-f), homogeneous geology model (m-n), double permeability model (u-v), and quadruple permeability model (cc-dd); total transpiration partitioning ratio averaged over the pre-drought period and the drought period for the free-draining model (g-h), homogeneous geology model (o-p), double permeability model (w-x), and quadruple permeability model (ee-ff).

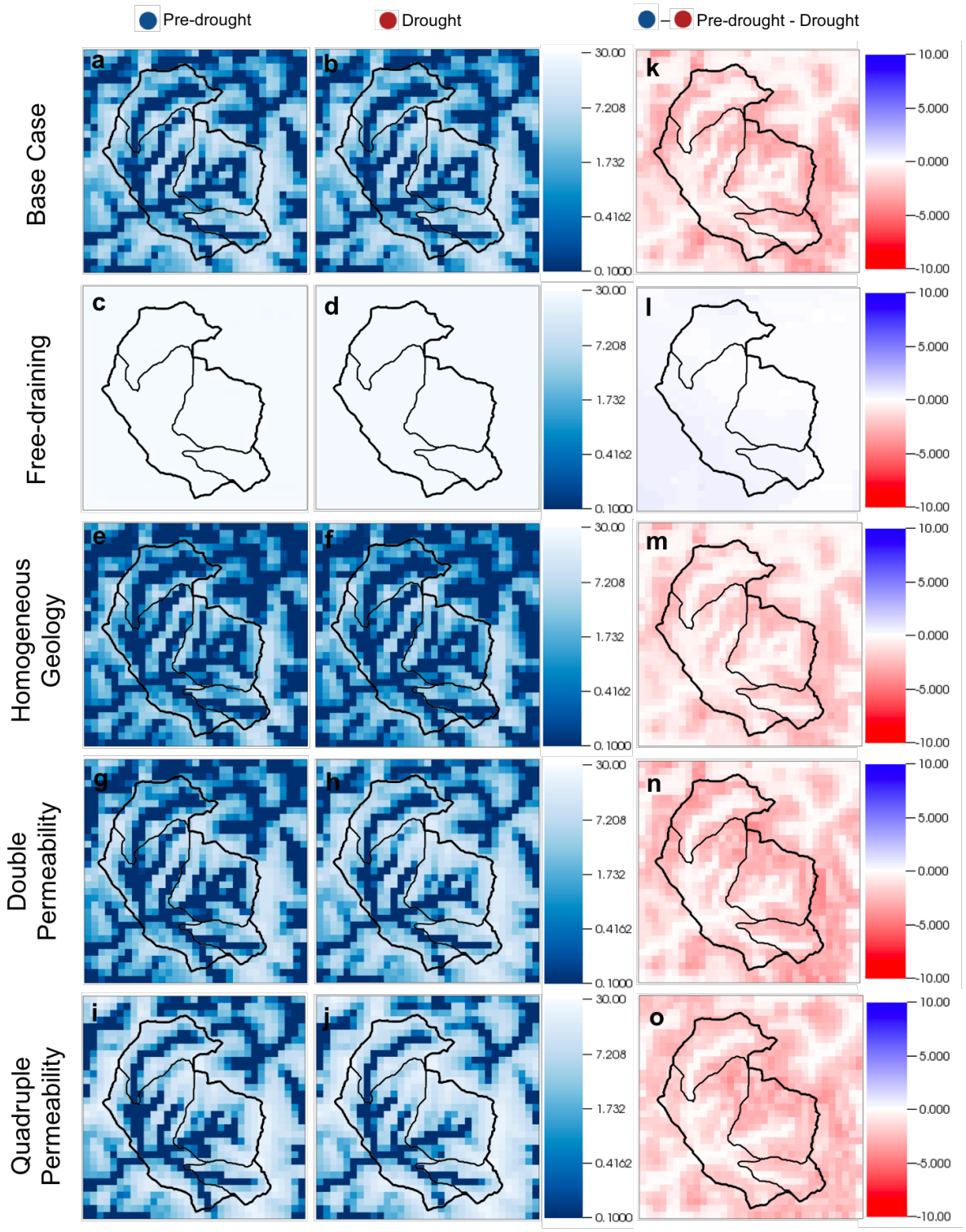


Figure A.4 Total annual average water table depth (WTD) for subsurface sensitivity study: the pre-drought and drought periods (a-j) and how the WTD changes during the drought (k-o) for all model characterizations, where dark blue indicates more water/shallower water table depths (WTDs) and light blue indicates less water/deeper water table depths (WTDs).